particles

MDPI

Article

Gluon Propagators in QC_2D at High Baryon Density

Vitaly Bornyakov [1,2,3], Andrey Kotov [2,4], Aleksandr Nikolaev [5] and Roman Rogalyov [1,*]

1 NRC "Kurchatov Institute"—IHEP, Protvino 142281, Russia; bornvit@gmail.com
2 NRC "Kurchatov Institute"—ITEP, Moscow 117218, Russia; kotov.andrey.yu@gmail.com
3 School of Biomedicine, Far Eastern Federal University, Vladivostok 690950, Russia
4 Bogoliubov Laboratory of Theoretical Physics, Joint Institute for Nuclear Research, Dubna 141980, Russia
5 Department of Physics, College of Science, Swansea University, Swansea SA2 8PP, UK; nikolauev@gmail.com
* Correspondence: rnr@ihep.ru

Received: 15 December 2019; Accepted: 23 March 2020; Published: 1 April 2020

Abstract: We study the transverse and longitudinal gluon propagators in the Landau-gauge lattice QCD with gauge group $SU(2)$ at nonzero quark chemical potential and zero temperature. We show that both propagators demonstrate substantial dependence on the quark chemical potential. This observation does not agree with earlier findings by other groups.

Keywords: lattice QCD; baryon density; gluon propagator; screening mass

1. Introduction

The properties of nuclear matter at low temperature and high density and the location of the phase transition to deconfined quark matter are subjects of both experimental and theoretical studies. It is known that the non-perturbative first principles approach as lattice QCD is inapplicable at large baryon densities and small temperatures due to the so-called sign problem. This makes important to study the QCD-like models [1], in particular lattice $SU(2)$ QCD (also called QC_2D). The properties of this theory were studied with the help of various approaches—chiral perturbation theory [1–3], Nambu-Jona-Lasinio model [4–6], quark-meson-diquark model [7,8], random matrix theory [9,10]. Supported by agreement with high precision lattice results obtained in SU(2) QCD these methods can be applied to real QCD with higher confidence. Lattice studies were made with staggered fermions [11–18] for $N_f = 4$ or, more recently, $N_f = 2$ and Wilson fermions [19–24] for $N_f = 2$ mostly.

The phase structure of $N_f = 2$ QC_2D at large baryon density and $T = 0$ was studied recently in Reference [16]. The simulations were carried out at small lattice spacing and the range of large quark chemical potential was reached without large lattice artifacts. The main result of Reference [16] is the observation that the string tension σ is compatible with zero for μ_q above 850 MeV. It was also found that the so called spatial string tension σ_s started to decrease at approximately same value of μ_q and went to zero at $\mu_q > 2000$ MeV.

The gluon propagators are among important quantities, for example, they play crucial role in the Dyson-Schwinger equations approach and other approaches [25–28].

In this paper we present results of our study of dependence of the gluon propagators and respective screening masses on μ_q, including large μ_q values range. We also look for signals of the confinement-deconfinement transition in the propagator behavior.

Landau gauge gluon propagators were extensively studied in the infrared range of momenta by various methods. We shall note lattice gauge theory, Dyson-Schwinger equations, Gribov-Zwanziger approach. At the same time the studies in the particular case of nonzero quark chemical potential are restricted to a few papers only. For the lattice QCD this is explained by the sign problem mentioned above.

The gluon propagators in lattice QC_2D at zero and nonzero μ_q were studied for the first time in [20]. This study was continued in [24,29,30].

The main conclusion of Reference [24] was that the gluon propagators practically do not change for the range of μ_q values studied: $\mu_q < 1.1$ GeV. The main conclusion of this paper is opposite: we found substantial influence of the quark chemical potential on the gluon propagators starting from rather low values ($\mu_q \sim 300$ MeV) and increasing with increasing μ_q. Thus results presented in Reference [24] differ from our results presented in this paper in many respects. The reason for these rather drastic differences might be that the lattice action and lattice spacing differ from those used in our study.

2. Lattice Setup

For numerical simulations we used the tree level improved Symanzik gauge action [31] and the staggered fermion action of the form

$$S_F = \sum_{x,y} \bar{\psi}_x M(\mu, m)_{x,y} \psi_y + \frac{\lambda}{2} \sum_x \left(\psi_x^T \tau_2 \psi_x + \bar{\psi}_x \tau_2 \bar{\psi}_x^T \right), \tag{1}$$

with

$$M(\mu, m)_{xy} = ma\delta_{xy} + \frac{1}{2} \sum_{\nu=1}^{4} \eta_\nu(x) \left[U_{x,\nu} \delta_{x+h_\nu,y} e^{\mu a \delta_{\nu,4}} - U^\dagger_{x-h_\nu,\nu} \delta_{x-h_\nu,y} e^{-\mu a \delta_{\nu,4}} \right], \tag{2}$$

where $\bar{\psi}$, ψ are staggered fermion fields, a is the lattice spacing, m is the bare quark mass, and $\eta_\nu(x)$ are the standard staggered phase factors. The quark chemical potential μ is introduced into the Dirac operator (2) through the multiplication of the lattice gauge field components $U(x,4)$ and $U^\dagger(x,4)$ by factors $e^{\pm \mu a}$, respectively.

We have to add to the standard staggered fermion action a diquark source term [11]. This term explicitly violates $U_V(1)$ symmetry and allows to observe diquark condensation on finite lattices, because this term effectively chooses one vacuum from the family of $U_V(1)$-symmetric vacua. Typically one carries out numerical simulations at a few nonzero values of the parameter λ and then extrapolates to $\lambda = 0$. The lattice configurations we are using were generated at one small value $\lambda = 0.00075$ which is much smaller than the quark mass in lattice units.

Integrating out the fermion fields, the partition function for the theory with the action $S = S_G + S_F$ can be written in the form

$$Z = \int DU e^{-S_G} \cdot Pf \begin{pmatrix} \lambda\tau_2 & M \\ -M^T & \lambda\tau_2 \end{pmatrix} = \int DU e^{-S_G} \cdot \left(\det(M^\dagger M + \lambda^2) \right)^{\frac{1}{2}}, \tag{3}$$

which corresponds to $N_f = 4$ dynamical fermions in the continuum limit. Note that the pfaffian Pf is strictly positive, thus one can use Hybrid Monte-Carlo methods to compute the integral. First lattice studies of the theory with partition function (3) have been carried out in References [12–14]. We study a theory with the partition function

$$Z = \int DU e^{-S_G} \cdot \left(\det(M^\dagger M + \lambda^2) \right)^{\frac{1}{4}}, \tag{4}$$

corresponding to $N_f = 2$ dynamical fermions in the continuum limit.

We carry out our study using 32^4 lattices for a set of the chemical potentials in the range $a\mu_q \in (0, 0.3)$. These are the same configurations as were used in Reference [16].

At zero density scale was set using the QCD Sommer scale value $r_0 = 0.468(4)$ fm [32]. We found [16] $r_0/a = 10.6(2)$. Thus lattice spacing is $a = 0.044(1)$ fm while the string tension at $\mu_q = 0$ is $\sqrt{\sigma_0} = 476(5)$ MeV. The pion is rather heavy with its mass $m_\pi = 740(40)$ MeV. Similar values for the pion mass were used in Reference [24] as well as in earlier studies. The dependence of the gluon

propagators on the pion mass in QC_2D was not investigated so far. This important issue will be a subject of our future studies.

We employ the standard definition of the lattice gauge vector potential $A_{x,\mu}$ [33]:

$$A_{x,\mu} = \frac{Z}{2iag}\left(U_{x\mu} - U^{\dagger}_{x\mu}\right) \equiv A^{a}_{x,\mu}\frac{\sigma_a}{2}\,, \tag{5}$$

where Z is the renormalization factor. The lattice Landau gauge fixing condition is

$$(\nabla^B A)_x \equiv \frac{1}{a}\sum_{\mu=1}^{4}\left(A_{x,\mu} - A_{x-a\hat{\mu},\mu}\right) = 0\,, \tag{6}$$

which is equivalent to finding an extremum of the gauge functional

$$F_U(\omega) = \frac{1}{4V}\sum_{x\mu}\frac{1}{2}\ \mathrm{Tr}\ U^{\omega}_{x\mu}\,, \tag{7}$$

with respect to gauge transformations ω_x . To fix the Landau gauge we use the simulated annealing (SA) algorithm with subsequent overrelaxation [34]. To estimate the Gribov copy effect, we employed five gauge copies of each configuration; however, the difference between the "best-copy" and "worst-copy" values of each quantity under consideration lies within statistical errors.

The gluon propagator $D^{ab}_{\mu\nu}(p)$ is defined as follows:

$$D^{ab}_{\mu\nu}(p) = \frac{1}{Va^4}\langle \widetilde{A}^{a}_{\mu}(q)\widetilde{A}^{b}_{\nu}(-q)\rangle\,, \qquad \text{where} \qquad \widetilde{A}^{b}_{\mu}(q) = a^4\sum_{x}A^{b}_{x,\mu}\exp\Big(\,iq(x+\frac{\hat{\mu}a}{2})\Big), \tag{8}$$

$q_i \in (-N_s/2, N_s/2]$, $q_4 \in (-N_t/2, N_t/2]$ and the physical momenta p_μ are defined by the relations $ap_i = 2\sin(\pi q_i/N_s)$, $ap_4 = 2\sin(\pi q_4/N_t)$.

At nonzero μ_q the $O(4)$ symmetry is broken and there are two tensor structures for the gluon propagator [35] :

$$D^{ab}_{\mu\nu}(p) = \delta_{ab}\left(P^{T}_{\mu\nu}(p)D_T(p) + P^{L}_{\mu\nu}(p)D_L(p)\right)\,. \tag{9}$$

In what follows we consider the softest mode $p_4 = 0$ and use the notation $p = |\vec{p}|$ and $D_{L,T}(p) = D_{L,T}(0, |\vec{p}|)$. In this case, (symmetric) orthogonal projectors $P^{T;L}_{\mu\nu}(p)$ are defined as follows:

$$P^{T}_{ij}(p) = \left(\delta_{ij} - \frac{p_i p_j}{\vec{p}^2}\right), \quad P^{T}_{\mu 4}(p) = 0\,; \quad P^{L}_{44}(p) = 1\,; \ P^{L}_{\mu i}(p) = 0\,. \tag{10}$$

Therefore, two scalar propagators - longitudinal $D_L(p)$ and transverse $D_T(p)$ - are given by

$$D_T(p) = \begin{cases} \frac{1}{6}\sum_{a=1}^{3}\sum_{i=1}^{3}D^{aa}_{ii}(p) & \text{if} \quad p \neq 0 \\ \frac{1}{9}\sum_{a=1}^{3}\sum_{i=1}^{3}D^{aa}_{ii}(p) & \text{if} \quad p = 0 \end{cases}\,, \qquad D_L(p) = \frac{1}{3}\sum_{a=1}^{3}D^{aa}_{44}(p)\,,$$

$D_T(p)$ is associated with the magnetic sector, $D_L(p)$ – with the electric sector.

3. Gluon Propagators and Screening Masses

We begin with the analysis of the propagators in the infrared domain where their behavior is conventionally described in terms of the so called screening masses.

3.1. Definition of the Screening Mass

In the studies of the gluon propagators at finite temperatures/densities two definitions of the gluon screening mass are widely used. The first definition is as follows: chromoelectric(magnetic)

screening mass is the parameter $\tilde{m}$ that appears in the Taylor expansion of the respective (longitudinal or transverse) propagator at zero momentum (see References [36,37])

$$D^{-1}_{L,T}(p) = \zeta(\tilde{m}^2_{E,M} + p^2 + \bar{o}(p^2)) \; . \tag{11}$$

The second one was proposed by A.Linde [38] for high orders of finite-temperature perturbation theory to make sense, it has the form

$$m^2_M = \frac{1}{D_T(p=0)} \; . \tag{12}$$

Analogous quantity in the chromoelectric sector

$$m^2_E = \frac{1}{D_L(p=0)} \tag{13}$$

is often referred to as the chromoelectric screening mass [39]. These masses can be related by the factor ζ,

$$m^2_{E,M} = \zeta \tilde{m}^2_{E,M} \; . \tag{14}$$

If ζ is independent of the thermodynamic parameters, two definitions can be considered as equivalent (they differ by a constant factor and thermodynamic information is contained only in the dependence on the parameters). However, this is not always the case. To discriminate between them, we will label the former mass $\tilde{m}_{E,M}$ as the proper screening mass and the latter $m_{E,M}$ as the Linde screening mass.

We consider both masses in our study. Similar approach was used in Reference [37].

3.2. Screening Masses in QC_2D

We make fits over the extended range of momenta $p < p_{cut} = 2.3$ GeV, comparatively high momenta are allowed for because our minimal momentum is as big as $p_{min} = 0.88$ GeV.

We use the fit function

$$D^{-1}_L(p) = \zeta_E(\tilde{m}^2_E + p^2 + r_E \; p^4) \tag{15}$$

for the chromoelectric sector and

$$D^{-1}_T(p) = \zeta_M(\tilde{m}^2_M + p^2 + r_M \; p^4 + s_M \; p^6) \tag{16}$$

for the chromomagnetic sector. These fit functions and the cutoff momentum $p_{cut} = 2.3$ GeV are chosen for the following reasons: (i) fit function of the type (15) does not work for the transverse propagator: goodness-of-fit is not acceptable (typical p-value is of order 10^{-5}); (ii) it is unreasonable to use fit function of the type (16) in the chromoelectric sector because the parameters in this function are poorly determined, whereas satisfactory goodness-of-fit can be achieved with the 3-parameter fit; (iii) higher values of p_{cut} results in a decrease of goodness-of-fit, whereas lower values result in large errors in the parameters, however, at $\mu < 0.3$ GeV in the chromoelectric sector this is not the case and we choose $p_{cut} = 1.8$ GeV. An important argument for this choice is that the perturbative domain in the chromoelectric sector at $\mu < 0.3$ GeV involves momenta $\simeq 2$ GeV, see below.

We checked stability of the proper chromoelectric screening mass against an exclusion of zero momentum from our fit domain. At $\mu_q < 0.3$ GeV this procedure results in an increase of $\tilde{m}_E$ by more than two standard deviations, whereas at higher μ_q the value of $\tilde{m}_E$ changes within statistical errors.

As for the chromomagnetic screening mass, an exclusion of zero momentum results in a dramatic increase of its uncertainty. Thus the longitudinal propagator considered over the momentum range $0.8 < p < 2.3$ GeV does involve an information on the respective screening mass, whereas the transverse propagator — does not.

The dependence of both $\tilde{m}_E$ and m_E on the quark chemical potential is depicted in Figure 1, left panel. It is seen that at $\mu_q < 0.3$ GeV the difference between $\tilde{m}_E$ and m_E is greater than that at larger values of μ_q. At $\mu_q > 0.3$ GeV the ratio $\dfrac{\tilde{m}_E(\mu_q)}{m_E(\mu_q)} = \eta_E(\mu_q)$ depends only weakly on μ_q: the fit of $\eta_E(\mu_q)$ to a constant gives $\bar{\eta}_E = 1.6(1)$, $\dfrac{\chi^2}{N_{d.o.f}} = 0.51$ at $N_{d.o.f} = 9$ and the corresponding $p-$value equals to 0.87. One can see that $\tilde{m}_E$ and m_E show a qualitatively similar dependence on μ_q.

In the left panel of Figure 1 we also show the function

$$\tilde{m}_E \simeq c_0 + c_2\mu_q^2 \tag{17}$$

fitted to our values of $\tilde{m_E}$ with parameters $c_0 = 0.74(3)$ GeV, $c_2 = 0.57(6)$ GeV^{-1} and $\dfrac{\chi^2}{N_{d.o.f}} = 1.59$.

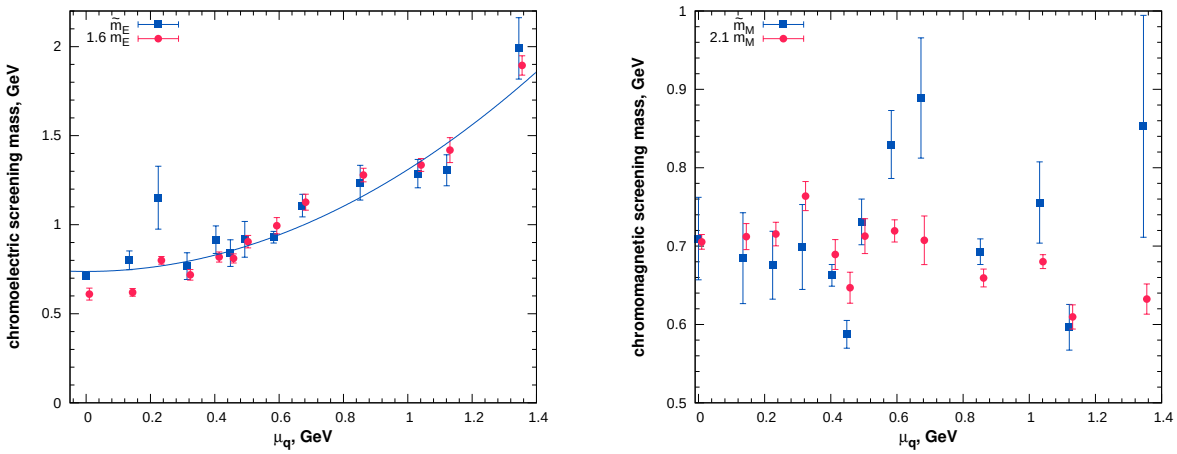

Figure 1. Chromoelectric (**left**) and chromomagnetic (**right**) Linde and proper screening masses as functions of μ_q. The Linde mass m_E is obtained from the propagators normalized at 6 GeV; to compare its dependence on μ_q with that of $\tilde{m}_E$, we show $1.6m_E$ for the chromoelectric mass and $2.1m_M$ for the chromomagnetic mass.

As in the chromoelectric case, the chromomagnetic ratio $\eta_M(\mu_q) = \dfrac{\tilde{m}_M(\mu_q)}{m_M(\mu_q)}$ can be fitted to a constant $\bar{\eta}_M = 2.1(1)$ with $\dfrac{\chi^2}{N_{d.o.f}} = 2.08$ at $N_{d.o.f} = 12$ and the corresponding $p-$value equals to 0.015. Thus we cannot draw a definite conclusion on the equivalence between chromomagnetic proper and Linde screening masses see Figure 1, right panel. Moreover, as was mentioned above, discarding zero momentum we lose substantial part of information on the infrared behavior of the transverse propagator. For this reason, the proper magnetic screening mass can hardly be reliably extracted from our data. The dependence of the chromomagnetic Linde screening mass on μ_q is shown in greater detail in Figure 2 together with the chromoelectric Linde screening mass.

Our results on the dependence of Linde screening masses on μ_q are in sharp disagreement with the results of Reference [24]. It was found in Reference [24] that at $a = 0.138$ fm m_M increases by some 20% when μ_q increases from 0 to 1.2 GeV and much faster growth was found at $a = 0.186$ fm. In opposite, we observe a trend to decreasing of the magnetic Linde screening mass with increasing μ_q. The chromoelectric screening mass in Reference [24] increases with μ_q at $a = 0.186$ fm and fluctuates about a constant on a finer lattice with $a = 0.138$ fm. We find that on our lattices with much smaller lattice spacing $a = 0.044$ fm m_E increases fast and this growth can be described by μ_q^2 behavior predicted by the perturbation theory. From the results in Reference [24] it follows that the chromoelectric and chromomagnetic screening masses come close to each other at all values of μ_q, whereas we find that

they coincide only at $\mu_q = 0$ and come apart from each other as μ_q increases. Thus lattices with spacing $a > 0.13$ fm used in Reference [24] might be not sufficiently fine for the studies of screening masses. The reason may stem from the fact that the condition $\mu_q \ll \frac{1}{a}$ does not hold at large values of μ_q on such coarse lattices. Therewith, to study the gluon propagators in the infrared region one needs large physical volume. As a compromise between these two requirements we choose $L = 32a = 1.4$ fm, having regard to a potential problem of finite volume effects at small momenta. Thus the validity of our results at larger volumes should be discussed in more detail.

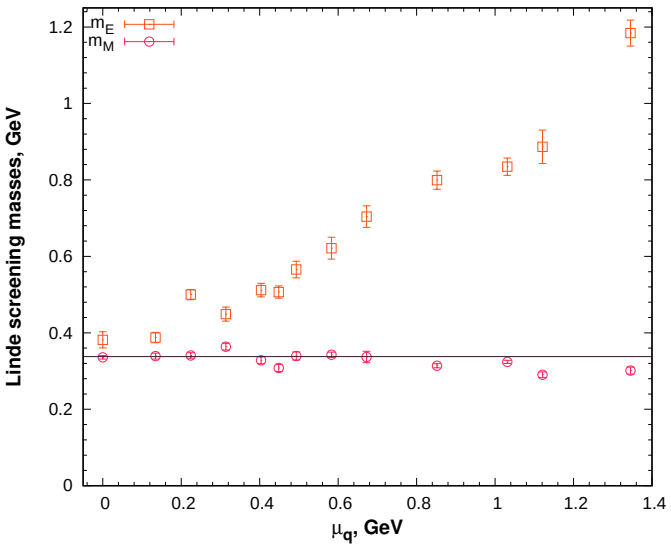

Figure 2. Chromoelectric m_E and chromomagnetic m_M Linde screening masses as functions of μ_q. Horizontal line results from the fit of the data on the Linde mass to a constant over the range $0 < p < 0.75$ GeV: it is seen that at higher μ_q the Linde chromomagnetic screening mass tends to decrease, in contrast to the results obtained in Reference [24].

In the $SU(2)$ gluodynamics at $T = 0$ it was shown [34,40,41] that the finite volume effects for the gluon propagator are substantially reduced when the invariance of the action under Z_2 nonperiodic gauge transformations (also referred to as Z_2 flips) is broken by picking up the flip sector with the highest gauge fixing functional. It was shown that the finite volume effects practically disappear already at the minimal nonzero momentum and reduce substantially at zero momentum [34,40,41].

In a theory with fermions Z_2 symmetry is explicitly broken by the matter field. Then it is natural to expect that the volume dependence of the gluon propagator is similar to that of gluodynamics with the improved gauge fixing of References [34,40,41].

Unfortunately, our expectations were not checked so far: volume dependence of the gluon propagator in theories with fermions have received only little attention, we know only one work on this problem [42], where close vicinity of pseudocritical temperature was investigated. It was observed in this work (see the Figures 1 and 2) that the volume dependence for the minimal momentum is small and is invisible for higher momenta. Still at the moment there is no clear understanding of the volume dependence of the gluon propagators in the case under consideration ($T = 0, \mu_q$ varies).

In the case of the longitudinal propagator $D_L(p)$, some evidence for the validity of our results at larger volumes comes from the following reasoning. At sufficiently high density the chromoelectric screening length determined as the inverse of the chromoelectric mass can be evaluated in perturbation theory, $l_E = \frac{1}{m_E} \sim \frac{1}{g(\mu_q)\mu_q}$. Our results are in agreement with this prediction. Thus we expect that with increasing μ_q the finite volume effects for this propagator should decrease.

At the same time the screening length associated with the transverse propagator $D_T(p)$ is defined as the inverse of the chromomagnetic screening mass $\tilde{m}_M$. Perturbation theory predicts $\tilde{m}_M = 0$ at high μ_q [43]; for this reason we should use nonperturbative estimates of m_M. On these grounds we expect that at sufficiently high μ_q (where perturbation theory works) m_M goes down, the respective screening length becomes large, and to study the infrared behavior of $D_T(p)$ large lattices are needed.

However, not only the zero-momentum propagators but also the propagators at nonzero momenta depend on μ_q. Both longitudinal and transverse propagators for the first and second minimal nonzero momenta are shown as functions of μ_q in Figure 3. It is known from the gluodynamics studies that the finite-volume effects decrease fast with increasing momentum. In Reference [41] it was even found, though on the coarse lattice, that the finite volume effects exist only for zero momentum and disappear for any nonzero momentum when improved gauge fixing is applied. We expect similar dependence of the finite volume effects on momentum in QC_2D.

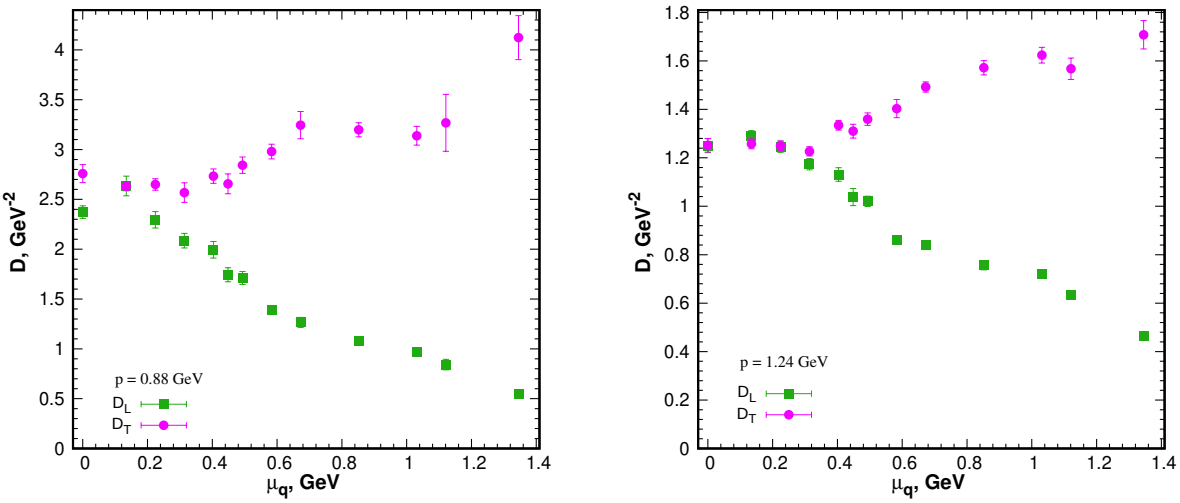

Figure 3. Gluon propagators as functions of μ_q at the minimal and next-to-minimal momenta.

It is seen that μ_q dependence of the transverse propagator at momenta $p \sim 1$ GeV, is even more pronounced than that at $p = 0$. The longitudinal propagator shows a similar μ_q dependence both at zero and minimal nonzero momenta. All these observations support our conclusion on substantial μ_q dependence of the gluon propagators in the infrared domain. Moreover, the longitudinal propagator decreases with increasing μ_q, whereas the transverse propagator increases.

4. Perturbative Behavior at High Momenta and Chemical Potentials

At sufficiently high momenta it is natural to expect the RG-modified perturbative behavior of the gluon propagator at all values of μ_q.

In the one loop approximation, the asymptotic behavior of the gluon dressing function $J(p) = D(p)p^2$ has the form

$$\lim_{p\to\infty; g=const} J(p;g) \simeq \left[\frac{\ln\left(\frac{p^2}{\Lambda^2}\right)}{\ln\left(\frac{\kappa^2}{\Lambda^2}\right)}\right]^{-c/(2b)}, \tag{18}$$

c and b are the coefficients of the RG functions,

$$\beta(g) \simeq -bg^3, \qquad \gamma(g) \simeq -cg^2 \tag{19}$$

and κ is the normalization point. In the Landau-gauge $SU(N_c)$ theories with N_F flavors [44] we arrive at

$$\frac{c}{2b} = \frac{13N_c - 4N_F}{2(11N_c - 2N_F)} = \frac{1}{2}. \tag{20}$$

Thus we fit our data to the function

$$J_{PT}(p) = \left[\frac{\ln\left(\frac{p^2}{\Lambda^2}\right)}{\ln\left(\frac{\kappa_0^2}{\Lambda^2}\right)}\right]^{-0.5}, \tag{21}$$

where $\kappa_0 = 6$ GeV, over the domain $p > p_{cut}$. The results are shown in Figure 4.

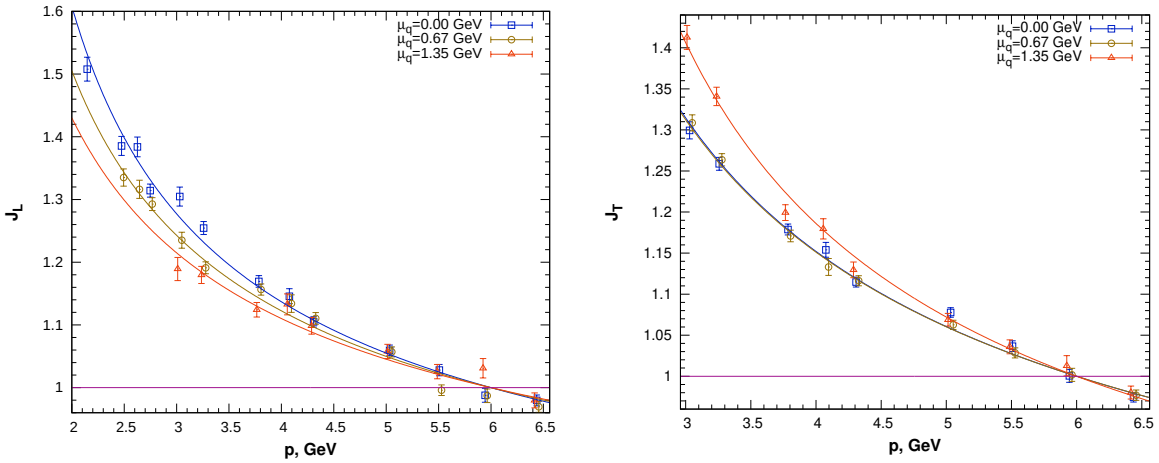

Figure 4. Longitudinal (left panel) and transverse (right panel) dressing functions at various values of μ_q. Curves are obtained with the fit function (21).

Goodness-of-fit is decreased by the effects of $O(3)$ symmetry breaking, however, we do not perform a systematic study of these effects assuming that making use of the asymptotic standard error in the fitting parameter Λ takes these effects into account.

Each value of the cutoff momentum p_{cut} is chosen so that (i) smaller values of p_{cut} result in a substantial decrease of the respective p-value and (ii) greater values of p_{cut} give no significant increase of the respective p-value. Thus we conclude that a domain of high momenta, where the longitudinal and transverse propagators can be described by the perturbatively motivated fit formula (21), does exist for each value of μ_q. In the transverse case, this domain is bounded from below by the cutoff momentum $p_{cut} = 2.9$ GeV irrespective of μ_q. In the longitudinal case, the cutoff momenta can be roughly approximated by the formula

$$p_{cut} = 1.8\text{GeV} + 1.0\mu_q\,. \tag{22}$$

The dependence of the resulting parameters on μ_q is shown in Figure 5. Λ_L and Λ_T designate the parameter Λ determined from the fit to J_L and J_T, respectively.

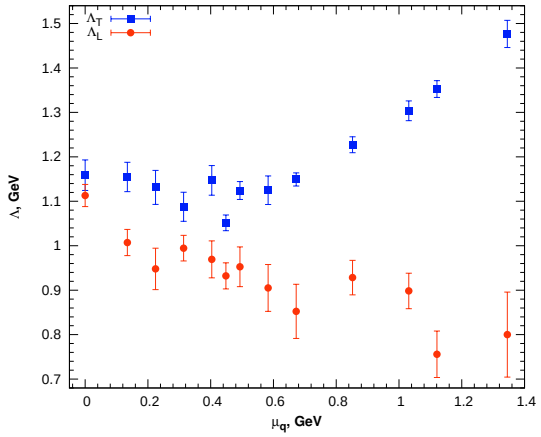

Figure 5. The parameter Λ from formula (21) for the transverse and longitudinal dressing functions.

Λ_L gradually decreases with increasing μ_q, whereas Λ_T remains constant at $\mu_q < \mu_q^b \sim 700 \div 800$ MeV and shows a linear dependence on μ_q,

$$\Lambda_T = \alpha_1 \mu_q + \alpha_0 \ , \tag{23}$$

at $\mu_q > \mu_q^b$. Fit over the range $\mu_q > 0.65$ GeV gives $\alpha_0 = 0.831(17)$ GeV and $\alpha_0 = 0.468(18)$ with $\chi^2/N_{d.o.f.} = 0.19$. Let us note that this sharp change in the behavior of $\Lambda_T(\mu_q)$ occurs at $\mu_q = \mu_q^b$, which is only a little smaller than the value $\mu_q^s \sim 850$ MeV, where σ_s starts to decrease (see Reference [16]). This value is also close to the chemical potential at which the string tension σ vanishes. Therefore, the high-momentum behavior of D_T changes in the deconfinement phase.

At $\mu_q > \mu_q^b$ the scale parameter Λ_T depends on the chemical potential and, if formula (23) holds true in the limit $\mu_q \to \infty$, then

$$\frac{\ln\left(\frac{p^2}{\Lambda_T^2}\right)}{\ln\left(\frac{\kappa_0^2}{\Lambda_T^2}\right)} \simeq \frac{\ln\left(\frac{p^2}{\alpha_1^2\mu_q^2}\right)}{\ln\left(\frac{\kappa_0^2}{\alpha_1^2\mu_q^2}\right)} \ .$$

That is, at sufficiently high μ_q the scale parameter in the expression for J_T is proportional to the chemical potential, as it is expected, whereas the scale parameter in the expression for J_L depends only weakly on μ_q. This controversial situation is very interesting and suggests further investigations.

5. Conclusions

We studied the gluon propagators in $N_f = 2$ $SU(2)$ QCD at $T = 0$ in the domain $0 < \mu_q < 1.4$ GeV, $0 < p < 6.5$ GeV. It was found that both longitudinal and transverse propagators depend on the chemical potential both at low and high momenta.

At low momenta, we describe this dependence in terms of the chromoelectric (m_E) and chromomagnetic (m_M) screening masses using two definitions: Linde screening masses $m_{E,M}$ and proper screening masses $\tilde{m}_{E,M}$. We found a good agreement between the two definitions of the chromoelectric screening mass at least at $\mu_q > 0.3$ GeV. m_E increases substantially with μ_q and can be fitted by the function (17).

The case of the chromomagnetic screening mass is more complicated: we find only a rough agreement between the two definitions. The Linde mass m_M can be evaluated more precisely; it depends only weakly on μ_q and can be fitted well by a constant at $\mu_q < 0.8$ GeV. At higher μ_q one can see decreasing of m_M which agrees with decreasing of σ_s. Results for higher values of μ_q are needed to decide whether m_M goes to zero at large μ_q as was argued in Reference [43]. In any case, the difference between m_E and m_M shows a substantial growth with μ_q starting at $\mu_q \approx 0.3$ GeV (see Figure 2).

It should be emphasized that our findings do not agree with the results of Reference [24], where it was concluded that *(i)* m_M comes close to m_E for all μ_q and *(ii)* both screening masses depend only weakly on μ_q.

However, since the physical lattice size used in our study is not large, $D_L(0)$ and $D_T(0)$ are potentially subject to finite-volume effects, see discussion between Figures 2 and 3.

At high momenta, we used the perturbatively motivated fit function (21) and described μ_q-dependence of the propagators $D_{T,L}$ in terms of the scaling parameters $\Lambda_{T,L}$ that appear in formulas like (21) for D_T and D_L.

Λ_L shows a slow decrease with increasing μ_q, whereas Λ_T =const at $\mu_q < 750$ MeV and shows a linear growth at higher values of μ_q. A sharp change in the behavior of $\Lambda_T(\mu_q)$ occurs at μ_q where the spatial string tension σ_s peaks (see Reference [16]).

Author Contributions: Conceptualization, R.R. and V.B.; Data curation, A.N.; Formal analysis, R.R. and A.K.; Investigation, R.R. and V.B.; Methodology, V.B. and A.K.; Project administration, V.B.; Software, A.K. and A.N.; Validation, A.K.; Visualization, R.R.; Writing—original draft, R.R.; Writing—review and editing, V.B. and A.N. All authors have read and agree to the published version of the manuscript.

Funding: The work was completed due to support of the Russian Foundation for Basic Research via grant 18-02-40130 mega (analysis of gluon propagators) and via grant 18-32-20172 (gauge fixing and Gribov copy effects analysis). A. A. N. acknowledges support from STFC via grant ST/P00055X/1.

Acknowledgments: The authors are grateful to V. V. Braguta for useful discussions. Computer simulations were performed on the IHEP (Protvino) Central Linux Cluster, ITEP (Moscow) Linux Cluster, the shared research facilities of HPC computing resources at Lomonosov Moscow State University, and the federal collective usage center Complex for Simulation and Data Processing for Mega-science Facilities at NRC "Kurchatov Institute", http://ckp.nrcki.ru/.

Conflicts of Interest: The authors declare no conflict of interest.

References

1. Kogut, J.B.; Stephanov, M.A.; Toublan, D.; Verbaarschot, J.J.M.; Zhitnitsky, A. QCD - like theories at finite baryon density. *Nucl. Phys. B* **2000**, *582*, 477. doi:10.1016/S0550-3213(00)00242-X. [CrossRef]
2. Splittorff, K.; Toublan, D.; Verbaarschot, J.J.M. Diquark condensate in QCD with two colors at next-to-leading order. *Nucl. Phys. B* **2002**, *620*, 290. doi:10.1016/S0550-3213(01)00536-3. [CrossRef]
3. Kanazawa, T.; Wettig, T.; Yamamoto, N. Chiral Lagrangian and spectral sum rules for dense two-color QCD. *JHEP* **2009**, *908*, 003. doi:10.1088/1126-6708/2009/08/003. [CrossRef]
4. Brauner, T.; Fukushima, K.; Hidaka, Y. Two-color quark matter: U(1)(A) restoration, superfluidity, and quarkyonic phase. *Phys. Rev. D* **2009**, *80*, 074035.; Erratum: [*Phys. Rev. D* **2010**, *81*, 119904]. doi:10.1103/PhysRevD.80.074035. [CrossRef]
5. Sun, G.f.; He, L.; Zhuang, P. BEC-BCS crossover in the Nambu-Jona-Lasinio model of QCD. *Phys. Rev. D* **2007**, *75*, 096004. doi:10.1103/PhysRevD.75.096004. [CrossRef]
6. He, L. Nambu-Jona-Lasinio model description of weakly interacting Bose condensate and BEC-BCS crossover in dense QCD-like theories. *Phys. Rev. D* **2010**, *82*, 096003. doi:10.1103/PhysRevD.82.096003. [CrossRef]
7. Strodthoff, N.; Schaefer, B.J.; von Smekal, L. Quark-meson-diquark model for two-color QCD. *Phys. Rev. D* **2012**, *85*, 074007. doi:10.1103/PhysRevD.85.074007. [CrossRef]
8. Strodthoff, N.; von Smekal, L. Polyakov-Quark-Meson-Diquark Model for two-color QCD. *Phys. Lett. B* **2014**, *731*, 350. doi:10.1016/j.physletb.2014.03.008. [CrossRef]
9. Vanderheyden, B.; Jackson, A.D. Random matrix study of the phase structure of QCD with two colors. *Phys. Rev. D* **2001**, *64*, 074016. doi:10.1103/PhysRevD.64.074016. [CrossRef]
10. Kanazawa, T.; Wettig, T.; Yamamoto, N. Singular values of the Dirac operator in dense QCD-like theories. *JHEP* **2011**, *1112*, 007. doi:10.1007/JHEP12(2011)007. [CrossRef]
11. Hands, S.; Kogut, J.B.; Lombardo, M.P.; Morrison, S.E. Symmetries and spectrum of SU(2) lattice gauge theory at finite chemical potential. *Nucl. Phys. B* **1999**, *558*, 327. doi:10.1016/S0550-3213(99)00364-8. [CrossRef]
12. Kogut, J.B.; Sinclair, D.K.; Hands, S.J.; Morrison, S.E. Two color QCD at nonzero quark number density. *Phys. Rev. D* **2001**, *64*, 094505. doi:10.1103/PhysRevD.64.094505. [CrossRef]

13. Kogut, J.B.; Toublan, D.; Sinclair, D.K. Diquark condensation at nonzero chemical potential and temperature. *Phys. Lett. B* **2001**, *514*, 77. doi:10.1016/S0370-2693(01)00586-X. [CrossRef]
14. J. B. Kogut, D. Toublan and D. K. Sinclair, The Phase diagram of four flavor SU(2) lattice gauge theory at nonzero chemical potential and temperature. *Nucl. Phys. B* **2002**, *642*, 181. doi:10.1016/S0550-3213(02)00678-8. [CrossRef]
15. Braguta, V.V.; Ilgenfritz, E.; Kotov, A.Y.; Molochkov, A.V.; Nikolaev, A.A. Study of the phase diagram of dense two-color QCD within lattice simulation. *Phys. Rev. D* **2016**, *94*, 114510. doi:10.1103/PhysRevD.94.114510. [CrossRef]
16. Bornyakov, V.G.; Braguta, V.V.; Ilgenfritz, E.-.; Kotov, A.Y.; Molochkov, A.V.; Nikolaev, A.A. Observation of deconfinement in a cold dense quark medium. *JHEP* **2018**, *1803*, 161. doi:10.1007/JHEP03(2018)161. [CrossRef]
17. Astrakhantsev, N.Y.; Bornyakov, V.G.; Braguta, V.V.; Ilgenfritz, E.; Kotov, A.Y.; Nikolaev, A.A.; Rothkopf, A. Lattice study of static quark-antiquark interactions in dense quark matter. *JHEP* **2019**, *1905*, 171. doi:10.1007/JHEP05(2019)171. [CrossRef]
18. Wilhelm, J.; Holicki, L.; Smith, D.; Wellegehausen, B.; von Smekal, L. Continuum Goldstone spectrum of two-color QCD at finite density with staggered quarks. *Phys. Rev. D* **2019**, *100*, 114507, doi:10.1103/PhysRevD.100.114507. [CrossRef]
19. Nakamura, A. Quarks and Gluons at Finite Temperature and Density. *Phys. Lett.* **1984**, *149B*, 391, doi:10.1016/0370-2693(84)90430-1 [CrossRef]
20. Hands, S.; Kim, S.; Skullerud, J.I. Deconfinement in dense 2-color QCD. *Eur. Phys. J. C* **2006**, *48*, 193, doi:10.1140/epjc/s2006-02621-8. [CrossRef]
21. Hands, S.; Kim, S.; Skullerud, J.I. A Quarkyonic Phase in Dense Two Color Matter? *Phys. Rev. D* **2010**, *81*, 091502, doi:10.1103/PhysRevD.81.091502. [CrossRef]
22. Hands, S.; Kenny, P.; Kim, S.; Skullerud, J.I. Lattice Study of Dense Matter with Two Colors and Four Flavors. *Eur. Phys. J. A* **2011**, *47*, 60, doi:10.1140/epja/i2011-11060-1. [CrossRef]
23. Cotter, S.; Giudice, P.; Hands, S.; Skullerud, J.I. Towards the phase diagram of dense two-color matter. *Phys. Rev. D* **2013**, *87*, 034507, doi:10.1103/PhysRevD.87.034507. [CrossRef]
24. Boz, T.; Hajizadeh, O.; Maas, A.; Skullerud, J.I. Finite-density gauge correlation functions in QC2D. *Phys. Rev. D* **2019**, *99*, 074514, doi:10.1103/PhysRevD.99.074514.

    [CrossRef]
25. Maris, P.; Roberts, C.D. Dyson-Schwinger equations: A Tool for hadron physics. *Int. J. Mod. Phys.* **2003**, *E12*, 297–365, doi:10.1142/S0218301303001326. [CrossRef]
26. Fischer, C.S. Infrared properties of QCD from Dyson-Schwinger equations. *J. Phys.* **2006**, *G32*, R253–R291. [CrossRef]
27. Eichmann, G.; Sanchis-Alepuz, H.; Williams, R.; Alkofer, R.; Fischer, C.S. Baryons as relativistic three-quark bound states. *Prog. Part. Nucl. Phys.* **2016**, *91*, 1–100, doi:10.1016/j.ppnp.2016.07.001. [CrossRef]
28. Biernat, E.P.; Gross, F.; Peña, M.T.A.; Leitão, S. Quark mass function from a one-gluon-exchange-type interaction in Minkowski space. *Phys. Rev.* **2018**, *D98*, 114033, doi:10.1103/PhysRevD.98.114033. [CrossRef]
29. Boz, T.; Cotter, S.; Fister, L.; Mehta, D.; Skullerud, J.-I. Phase transitions and gluodynamics in 2-colour matter at high density. *Eur. Phys. J.* **2013**, *87*, 1303–3223. [CrossRef]
30. Hajizadeh, O.; Boz, T.; Maas, A.; Skullerud, J.-I. Gluon and ghost correlation functions of 2-color QCD at finite density. *EPJ Web Conf.* **2018**, *175*, 07012. [CrossRef]
31. Weisz, P. Continuum Limit Improved Lattice Action for Pure Yang-Mills Theory. 1. *Nucl. Phys. B* **1983**, *212*, 1, doi:10.1016/0550-3213(83)90595-3. [CrossRef]
32. Bazavov, A.; Bhattacharya, T.; Cheng, M.; DeTar, C.; Ding, H.T.; Gottlieb, S.; Gupta, R.; Hegde, P.; Heller, U.M.; Karsch, F.; et al. The chiral and deconfinement aspects of the QCD transition. *Phys. Rev. D* **2012**, *85*, 054503, doi:10.1103/PhysRevD.85.054503. [CrossRef]
33. Mandula, J.E.; Ogilvie, M. The Gluon Is Massive: A Lattice Calculation of the Gluon Propagator in the Landau Gauge. *Phys. Lett.* **1987**, *B185*, 127. [CrossRef]
34. Bornyakov, V.G.; Mitrjushkin, V.K.; Muller-Preussker, M. SU(2) lattice gluon propagator: Continuum limit, finite-volume effects and infrared mass scale m(IR). *Phys. Rev. D* **2010**, *81*, 054503, doi:10.1103/PhysRevD.81.054503. [CrossRef]

35. Kapusta, J.I.; Gale, C. *Finite-Temperature Field Theory: Principles and Applications*; Cambridge University Press: Cambridge, UK, 2006. [CrossRef]
36. Bornyakov, V.G.; Mitrjushkin, V.K. SU(2) lattice gluon propagators at finite temperatures in the deep infrared region and Gribov copy effects. *Phys. Rev. D* **2011**, *84*, 094503. [CrossRef]
37. Dudal, D.; Oliveira, O.; Silva, P.J. High precision statistical Landau gauge lattice gluon propagator computation vs. the Gribov–Zwanziger approach. *Annals Phys.* **2018**, *397*, 351, doi:10.1016/j.aop.2018.08.019. [CrossRef]
38. Linde, A.D. Infrared Problem in Thermodynamics of the Yang-Mills Gas. *Phys. Lett.* **1980**, *96B*, 289, doi:10.1016/0370-2693(80)90769-8. [CrossRef]
39. Maas, A. Describing gauge bosons at zero and finite temperature. *Phys. Rept.* **2013**, *524*, 203, doi:10.1016/j.physrep.2012.11.002. [CrossRef]
40. Bornyakov, V.G.; Mitrjushkin, V.K.; Muller-Preussker, M. Infrared Behavior and Gribov Ambiguity in SU(2) Lattice Gauge Theory. *arXiv* **2009**, arXiv:0812.2761.
41. Bogolubsky, I.L.; Bornyakov, V.G.; Burgio, G.; Ilgenfritz, E.M.; Muller-Preussker, M.; Mitrjushkin, V.K. Improved Landau gauge fixing and the suppression of finite-volume effects of the lattice gluon propagator. *Phys. Rev. D* **2008**, *77*, 014504.; Erratum: [*Phys. Rev. D* **2008**, *77*, 039902] doi:10.1103/PhysRevD.77.039902. [CrossRef]
42. Bornyakov, V.G.; Mitrjushkin, V.K. Lattice QCD gluon propagators near transition temperature. *Int. J. Mod. Phys.* **2012**, *A27*, 1250050. [CrossRef]
43. Son, D.T. Superconductivity by long range color magnetic interaction in high density quark matter. *Phys. Rev.* **1999**, *D59*, 094019. [CrossRef]
44. Politzer, H.D. Asymptotic Freedom: An Approach to Strong Interactions. *Phys. Rept.* **1974**, *14*, 129. [CrossRef]